

REPORT

Literature Review of Methodologies for Vegetation Identification and Removal from UAV-Based Photogrammetric DSMs for the Waste Isolation Pilot Plant

(In Support of Project 2, Task 6: Hydrology Modeling for WIPP, Subtask 6.1: Digital Elevation Model and Hydrologic Network)

Prepared by Gisselle Gutierrez-Zuniga, DOE Fellow

Date submitted:

January 17, 2020

Principal Investigator:

Leonel E. Lagos, PhD, PMP®

Florida International University Collaborators:

Yan Zhou, PhD

Angelique Lawrence, MS, GISP®

Submitted to:

U.S. Department of Energy

Office of Environmental Management

Under Cooperative Agreement # DE-EM0000598



Applied Research Center
FLORIDA INTERNATIONAL UNIVERSITY

TABLE OF CONTENTS

INTRODUCTION.....	3
RELEVANT PUBLICATIONS.....	5
SUMMARY	41
REFERENCES	42

INTRODUCTION

FIU is assisting DOE-EM's Carlsbad Field Office (CBFO) and Pacific Northwest National Laboratory (PNNL) in developing a groundwater-basin model for the Waste Isolation Pilot Plant (WIPP) site using the Advanced Simulation Capability for Environmental Management (ASCEM) modeling toolset to assist DOE-EM improve the current understanding of the regional water balance, particularly the relation between Culebra recharge and the intense, episodic precipitation events typical of the monsoon. This relationship is essential for understanding the rate of propagation of the shallow dissolution front, and the impact of land-use changes around the WIPP facility on water levels in compliance-monitoring wells.

ASCEM is an open source processed based computational framework for prediction of contaminant fate and transport in natural and engineered systems across DOE sites. Currently, ASCEM is unable to account for land surface hydrology, which is essential for computing the water balance. The proposed work will therefore require coupling of a state-of-the-art open-source land surface model (LSM) with the groundwater models (GWMs) within the ASCEM toolbox to simulate three-dimensional, unsaturated and saturated water flow. A revision of the current site conceptual model will be necessary to couple surface water and groundwater processes, which requires a high resolution digital elevation model including channels and sink holes to account for surface water routing, and the development of a new mathematical model. A high-resolution (1-m/sub-meter) DEM of the WIPP region is not currently available, therefore FIU plans to develop a high-resolution digital elevation model (DEM) for the WIPP site and surrounding basins using photogrammetric methods to better capture the ground surface topography and local features. A high resolution DEM of the site will enable more accurate delineation and extraction of features such as drainage basins, brine lakes, channels, sink holes and discharge points and will also facilitate future creation of spatially-distributed soil and vegetation classes.

Due to the cost of acquiring and processing LiDAR data for DEM development, the use of unmanned aerial vehicles (UAVs) to acquire digital photos is becoming more common. However, UAV-based point clouds do not represent the bare earth surface as well as LiDAR. This literature review therefore serves to investigate various ground filtering and machine learning methodologies for vegetation identification and removal from UAV-based photogrammetric digital surface models (DSMs) in order to improve DEM accuracy. The use of UAV-based photogrammetric methods provides a more affordable approach for DEM development. In conjunction with the appropriate ground filtering or machine learning methodology, it can provide researchers with accurate representations of the bare earth for development of land surface and hydrological models. Coupling of a LSM with the ASCEM GWMs will lead to more accurate predictions of groundwater flow patterns in the WIPP region, including horizontal flow (e.g., potentiometric surface, flow direction, vertical flow into

transmissive units, and the effect of density on flow direction). With improved estimates of the spatial and temporal patterns of recharge to force the GWM, predictions of halite dissolution and propagation of the shallow dissolution front will be made possible and the potential impact on repository performance quantified.

RELEVANT PUBLICATIONS

FIU conducted a literature review of methodologies for vegetation removal from UAV-based photogrammetric DSM for the Waste Isolation Pilot Plant (WIPP) The following are some of the journal articles reviewed arranged in chronological order with the latest techniques first:

METHODOLOGIES FOR VEGETATION REMOVAL FROM UNMANNED AERIAL VEHICLE (UAV)-BASED PHOTOGRAMMETRIC DIGITAL SURFACE MODELS

COMPARING FILTERING TECHNIQUES FOR REMOVING VEGETATION FROM UAV-BASED PHOTOGRAMMETRIC POINT CLOUDS

Anders, N., Valente, J., Masselink, R., & Keesstra, S. (2019). Comparing Filtering Techniques for Removing Vegetation from UAV-Based Photogrammetric Point Clouds. Drones, 3(3), 61.

There are many methods used to process LiDAR-derived point clouds and classify vegetation points, but they are not applicable to point clouds derived with photogrammetry. The use of Structure-from-Motion (SfM) to generate digital elevation models (DEM), which can contain information below dense vegetation unlike aerial images, has increased over time but there has not been a formal comparison of existing methods to determine which is best considering different settings, locations, and DTM applications. Therefore, the goal of this study was to evaluate the performance of different vegetation filtering algorithms for SfM-obtained point clouds. The filtering algorithms evaluated and compared were: color-based filtering using an excessive greenness vegetation index (VI), Triangulated Irregular Networks (TIN) densification from LAStools, the standard method in Agisoft Photoscan, Iterative Surface Lowering (ISL), and a combination of ISL and VI methods.

Methodology

This study was conducted in the Guadalantin basin in the Mediterranean region where grasses and shrubs dominate.



Figure 1. The left image is the map view of the study area in the Guadalantin Basin near Lorca and Murcia, Spain. The right image shows the spatial distribution of ground control points and reference points.

A fixed wing Mavinci Sirius 1 Unmanned Aerial Vehicle (UAV) with a 1.6 m wingspan and mass of 2.6 kg was used to collect aerial images. The camera used was a Panasonic Lumix GX1 16 MP camera (focal length 20 mm, aperture F1.7, exposure time 1/1600). The average flight altitude is 100 meters which resulted in images with an average ground sample distance (GSD) of 2 cm. There were 15 ground control points (GCPs) well distributed throughout the area at relatively low, medium, and high locations. The GCPs were 80 x 80 cm orange textile rectangles with a 30 x 30 cm black textile square with a CD on top. The coordinates of the center of the CD were measured with a TopCon HiPer Pro GNSS RTK receiver. The flight lines were programmed for the images to have 85% overlap in flight direction and 60% side overlap. A point cloud was then created from the images using Agisoft Photoscan and configured to “aggressive depth filtering” for dense point cloud processing.

Filtering Based On Excessive Greenness Index

Point clouds can contain color values that can be used to classify points, such as using thresholds of absolute color values or via vegetation indices. Vegetation indices are used to classify image pixels with vegetation information from other pixels such as bare ground, infrastructure, or clouds. The most effective vegetation indices are based on green, red, red-edge, near infrared and/or infra-red bands, such as the Normalized Difference Vegetation Index (NDVI) and the Enhanced Vegetation Index (EVI), but light-weight UAVs with a basic camera equipped with CMOS sensors are sensitive to visible light until near-infrared (NIR) (400-900 nm) with RGB channels and filters that block any radiation above 650 nm.

The Visible Vegetation Index (VVI) is an index between 0 and 1, where if the values are close to zero then it is bare ground and if the value are closer to 1 then it is vegetation. The following equation is used:

$$VVI = \left[\left(1 - \left| \frac{R - R_0}{R + R_0} \right| \right) \times \left(1 - \left| \frac{G - G_0}{G + G_0} \right| \right) \times \left(1 - \left| \frac{B - B_0}{B + B_0} \right| \right) \right]^{\frac{1}{w}}$$

where R, G, and B are the red, green, and blue channels, RGB_0 is the vector of the reference green color (this study used $R_0=40$, $G_0=60$, $B_0=10$), and w is the weight component (this study used $w=1$).

Excessive Greenness Index (ExG) is a continuous index where higher values indicate more green surfaces and low values indicating bare ground. The following formula is used:

$$ExG = 2G - R - B$$

This study calculated and visually compared the VVI and ExG and found that VVI was most useful when recognizing subtle differences between types of vegetation and with ExG there was a higher contrast between vegetation and bare ground. Because the point was to classify vegetation and bare ground, ExG was used. During filtering, any point with an $ExG > 0.1$ was removed from the point cloud.

TIN Densification

The TIN densification method is primarily based on the Triangular Irregular Networks where a sparse TIN is first created based on a minimum number of points. Next, points are iteratively added to the TIN to create a more detailed TIN, if the points meet certain criteria of the triangle within an established threshold. The threshold was established and updated after every iteration. Points in the TIN at the end of densification are accepted as a representation of the bare earth surface and the rest are classified as objects. The lowest points are the ones added to the triangulation and this retriangulation is repeated until no triangle has a point beneath it.

LAStools consists of a collection of command-line tools for processing point cloud data, including an implementation of ground point filtering using TIN densification. This study used LAStools, more specifically the `lasground_new.exe`, to filter ground points.

Agisoft Photoscan Native Filtering Algorithm

Agisoft Photoscan is a popular software product used to process aerial imagery and create point clouds, DEMs, and orthorectified mosaics which are used in this study. Agisoft includes a native implementation of ground point filtering that allows for threshold parameters which includes max angles between terrain and line to connect the point (15 degrees, higher values can improve results in steeper regions), max distance between terrain and a point (1 m), and cell size of the intermediate terrain (5 m, which is the max expected data gaps because of buildings and/or trees). Parameters were set based on which produced visually best results.

Iterative Surface Lowering (ISL)

ISL is similar to the TIN Densification method in that it iteratively changes a preliminary surface based on varying sets of points. First, all points are interpolated into a regularly gridded raster with a given cell size (1 m was chosen based on manual heuristics). All points above the surface are classified as vegetation points and points below are classified as ground points. The following iterations only include ground points to the surface interpolation. When there are no more points that change labels, the interpolated surface is assumed to represent ground surface.

ISL+VI

This method combines the ISL and ExG by removing vegetation points using the VI method and used the selection of ground points as the start for the ISL method.

Output

Each of the five test runs produced a classified point cloud and a number of rasters with 25 x 25 cm grid cells. If there were gaps, they were filled using Inverse Distance Weighting (IDW, $\text{weight} = 1/\text{distance}^2$) interpolation.

Error Assessment of Resulting DTMs

There were 15 reference points chosen for each vegetation category (bare ground, shrubs, and trees) and distributed throughout, totaling 45 reference points. To quantitatively assess the

results, an ANOVA test was used on the absolute error values per reference point per land cover class and if there were significant differences, the Tukey Honest Significance Difference (Tukey-HSD) test was used. To qualitatively assess the results, profiles were drawn on the DTMs to highlight the differences on a linear hillslope with alternating shrubs, a linear hillslope with alternating shrubs with a single tree, a channel surrounded by vegetation, a patch of trees and a hillslope with multiple patches of trees.

Results

Table 1. Number of points in point cloud per filter method and the percentage of the total amount of original points filters in each class. Root Mean Square Error (RMSE) showed for each land cover class.

	Ground	Vegetation	% Filtered	Bare	Shrub	Tree
DSM	3.20×10^7	0	0.00	0.05	0.96	5.16
ISL	2.40×10^7	0.79×10^7	24.83	0.05	0.31	3.04
ISL_VI	1.40×10^7	1.79×10^7	56.18	0.05	0.29	2.94
LOW	3.20×10^7	0	0.00	0.08	0.44	4.47
PS	3.00×10^7	0.19×10^7	6.06	0.05	0.50	0.81
TIN	2.07×10^7	1.13×10^7	35.41	0.05	0.33	0.78
VI	1.70×10^7	1.50×10^7	46.80	0.05	0.89	4.89

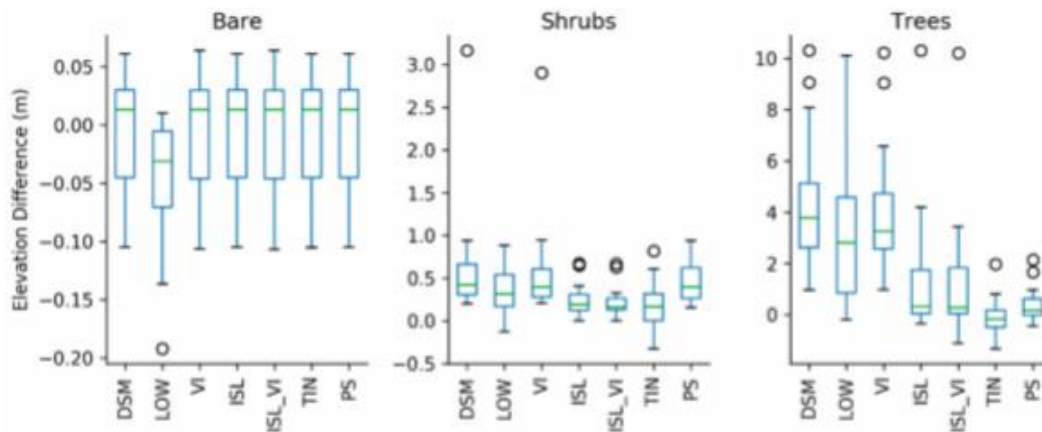


Figure 2. Boxplots for the three vegetation classes depicting the elevation differences between the reference points and the interpolated DTM after filtering.

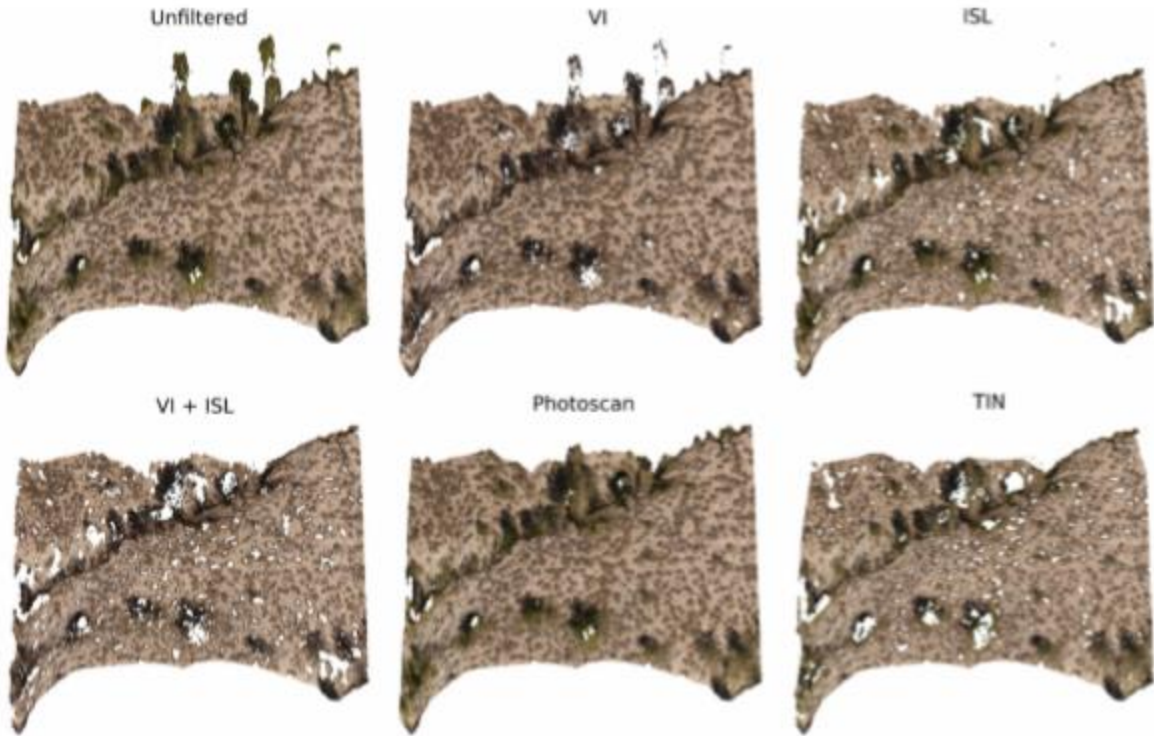


Figure 3. Colored point clouds showing the locations of the filtered vegetation points for a subset of area within the study area.

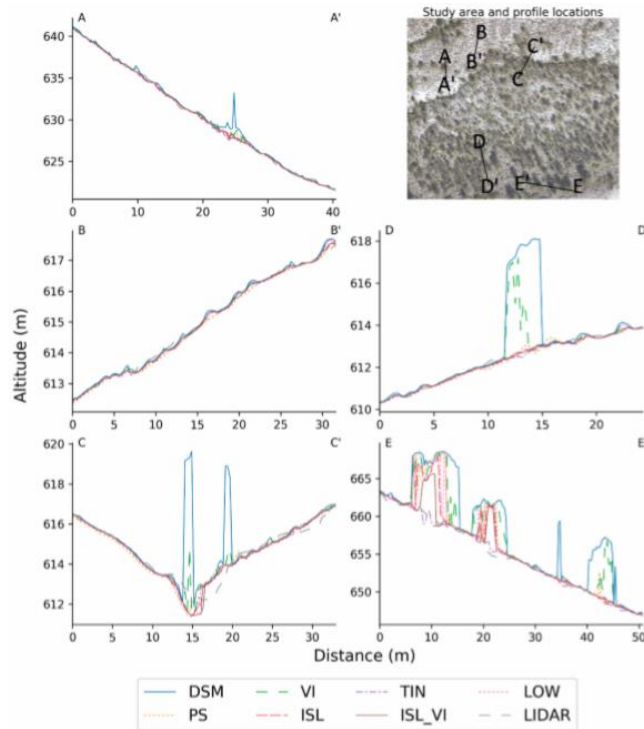


Figure 4. Profiles showing a similar image as the colored point clouds.

Conclusions

The study concluded that there was little to no difference between the filtering methods which can be explained by the fact that there was very little vegetation in the study area. For shrub and tree areas, the ISL, VI and TIN methods were concluded to be the best. It was determined that “off the shelf” algorithms are the best for vegetation removal and it is best to use more custom methods such as the TIN densification.

IMAGE CLASSIFICATION-BASED GROUND FILTERING OF POINT CLOUDS EXTRACTED FROM UAV-BASED AERIAL PHOTOS

Yilmaz, V., Konakoglu, B., Serifoglu, C., Gungor, O., & Gökalp, E. (2018). Image classification-based ground filtering of point clouds extracted from UAV-based aerial photos. Geocarto international, 33(3), 310-320.

Due to the cost of acquiring and processing LiDAR data, the use of unmanned aerial vehicles (UAVs) to acquire digital photos is becoming more common. However, UAV-based point clouds do not represent the bare earth surface as well as LiDAR. This study proposes a ground filtering methodology to filter UAV-based point clouds.

Support vector machines classification algorithm

The support vector machines (SVM) statistical learning theory separates classes with a decision surface (also known as an optimal hyperplane) maximizing the margin between the classes. Data points closest to the decision surface are ‘support vectors’. If the classes are linearly separable, then two parallel planes maximizing the margin between the classes are formed and an optimal hyper plane is placed in the middle of these parallel planes. Standard quadratic programming optimization techniques are used to maximize the margin between each class. If the classes cannot be linearly separated, each vector of a class is transformed into another higher dimensional space using a nonlinear transformation to increase the possibility of separating classes with a linear hyperplane.

Methodology

Two flights were conducted over the study area of the Karadeniz Technical University because the area was too large for just one flight. A Gatewing X100 UAV was used with a RICOH GR DIGITAL IV Digital Camera that was mounted on the UAV. The digital camera, which produces red, green, and blue bands, was calibrated before each flight. Twelve ground control points (GCPs) were established on the lower campus and 4 GCPs were placed in the upper campus. For the first flight, 256 aerial photos were taken from 185 m above along 9 flight paths while for the second flight, 160 aerial photos were taken from 175 m along 10 flight paths. After the flights, the images were processed on Agisoft Photoscan Professional software. Once imported onto Agisoft, the quality of each photo was analyzed and the low quality photos were removed because they could affect the alignment result. Next, a key point extraction was done photo by photo. Agisoft used the GCPs to georeference the point cloud produced after image matching and then calculated the 3D coordinates of the key points with automatic aerial triangulation. Next, a sparse point cloud with point density 0.5 point/m^2 was created. To create a high

resolution digital elevation model, the density of the created point cloud was increased using Agisoft. The software does this by calculating depth information for each camera and combines them into a single, dense point cloud based on the estimated camera positions. The resulting increased point cloud density was 152 point/m². Next, the generated point cloud was visually examined and it was found that there were points located too far from the study area and they were then deleted manually. The 3D mesh and model texture were then generated in the software to reconstruct the texture information. The final step was to produce a 10 cm orthophoto image of the study by processing the point cloud.

The ENVI software's SVM classifier was used to classify the orthophoto images taken into six classes: road, building, soil, grass, shadow, and tree; and red, green, and blue bands were used in the process. The classes road, grass, and soil were merged to generate the ground class. The classes building, shadow, and tree were merged to generate the non-ground class. The accuracy of the classified image was calculated with an error matrix and the McNemar test. Then, the classified image was overlapped with the generated point cloud to determine the points corresponding to the non-ground class. The determined non-ground points were then removed. The accuracy of the ground filtering process was determined using the Cohen's Kappa coefficient. The ground points were then interpolated to produce the DEM. To determine the vertical accuracy of the produced DEM, field measurements were conducted in four test sites.

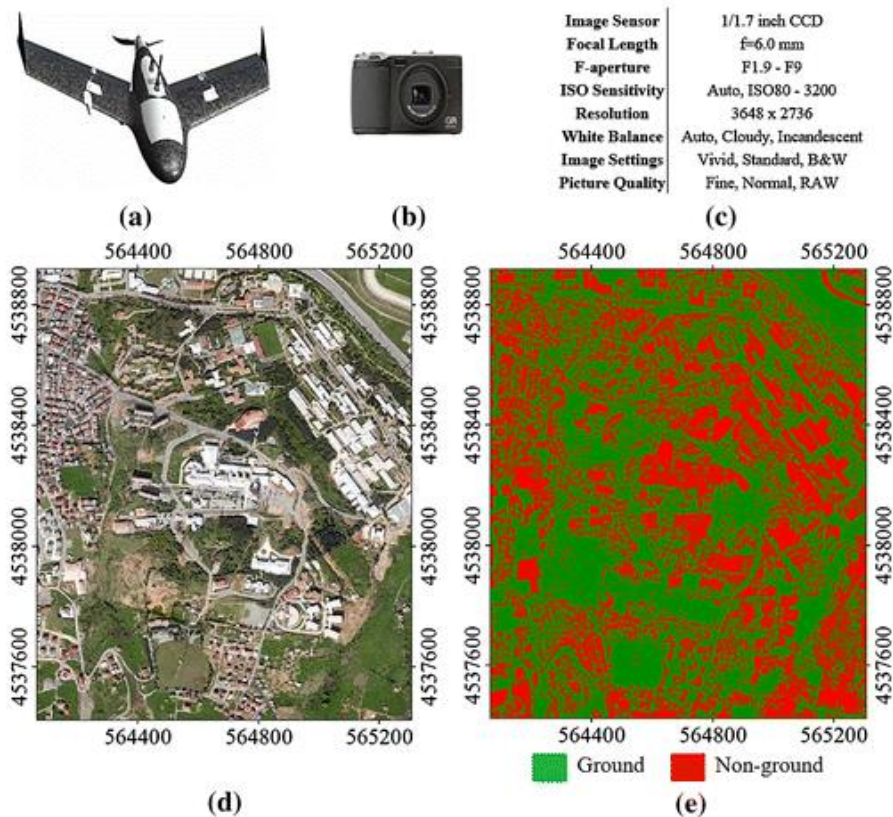


Figure 5. (a) Gatewing X100 UAV, (b) RICOH GR DIGITAL IV digital camera, (c) Technical specifications of the digital camera, (d) Orthophoto of the study area (10 cm), (e) Image produced with SVM classification algorithm

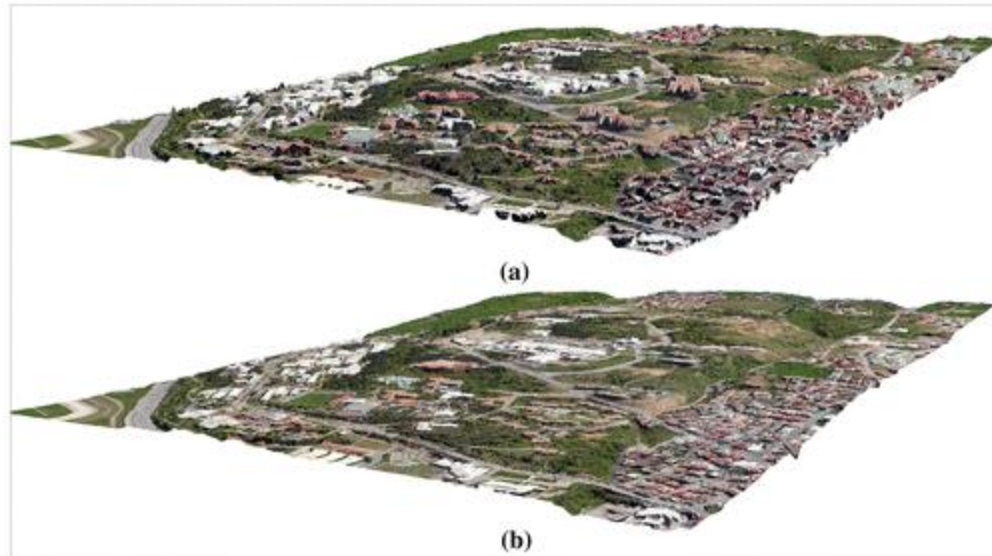


Figure 6. Orthophoto image draped over (a) DSM and (b) produced DEM

VEGETATION REMOVAL FROM UAV DERIVED DSMS, USING COMBINATION OF RGB AND NIR IMAGERY

Skarlatos, D., & Vlachos, M. (2018). Vegetation removal from UAV derived DSMS, using combination of RGB and NIR imagery.

The focus of this study was to create a detailed Digital Terrain Model (DTM) from drone aerial imagery by automatically filtering the vegetation on the Digital Surface Model (DSM) through standard control point acquisition.

Methodology

The methodology consisted of using NDVI to classify DSM points as vegetation and non-vegetation points, then using the non-vegetation points to create a DTM using interpolation to fill in any gaps that were created from the exclusion of the vegetation points. The high resolution multispectral imagery with 4 channels (red, green, blue, and near infrared) and a dense DSM were the inputs.

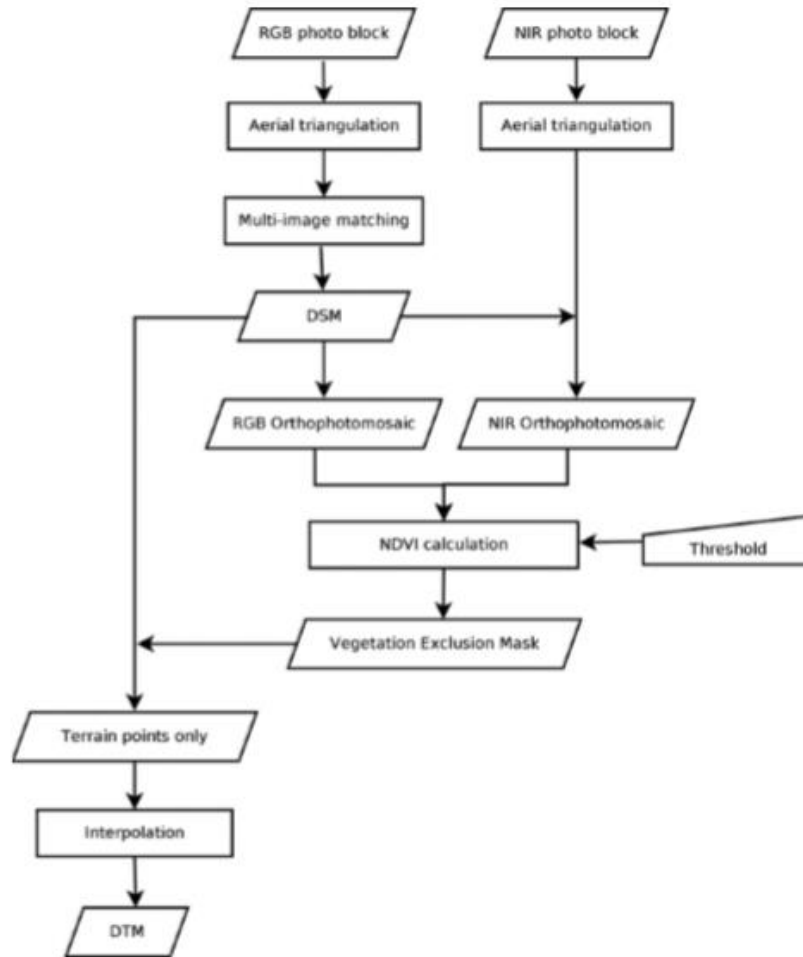


Figure 7. Diagram of methodology

The NDVI method was chosen and can be defined as:

$$NDVI = \frac{(NIR - RED)}{(NIR + RED)}$$

According to the study, the most common practice for NDVI calculation is to create two orthophotomosaics, an RGB and a NIR, and calculate the NDVI using the data from each orthophotomosaic. Once this is done, a threshold is defined for the mask creation. The threshold can be defined depending on illumination differences, vegetation type, topographic variations, sensor sensitivity, epoch, leaf coverage, etc. A low NDVI threshold can mask out valid ground points whereas a high threshold will include vegetation points and therefore worsen the accuracy. This study used a threshold of 0.09. Next, an interpolation algorithm was applied to fill in any gaps caused by the removal of vegetation points.

Study Area

Two areas were chosen for testing, based on the availability of GCPs among vegetation and bare ground. Two flights were done, one with the RGB camera and the other with the NIR camera.

The imagery collected was then processed on Agisoft Photoscan to create two orthophotos and a dense DSM.



Figure 8. Ground photos of Test Site A- Kimisala, Greece

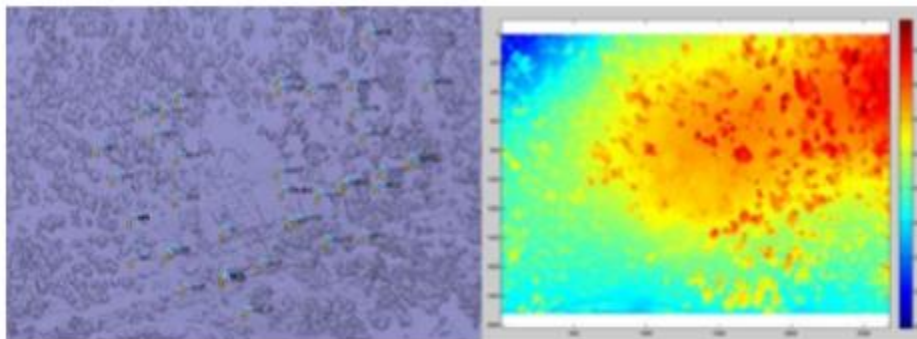


Figure 9. Test Site A DSM and GCPs

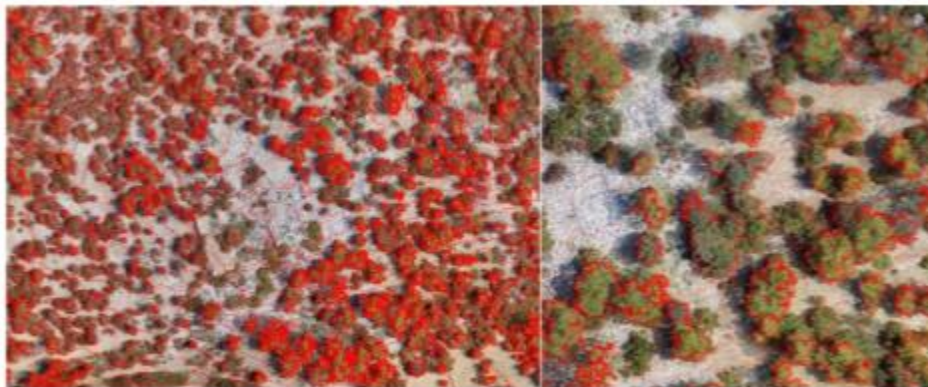


Figure 10. Test Site A orthophotomosaic, with 1 m contours

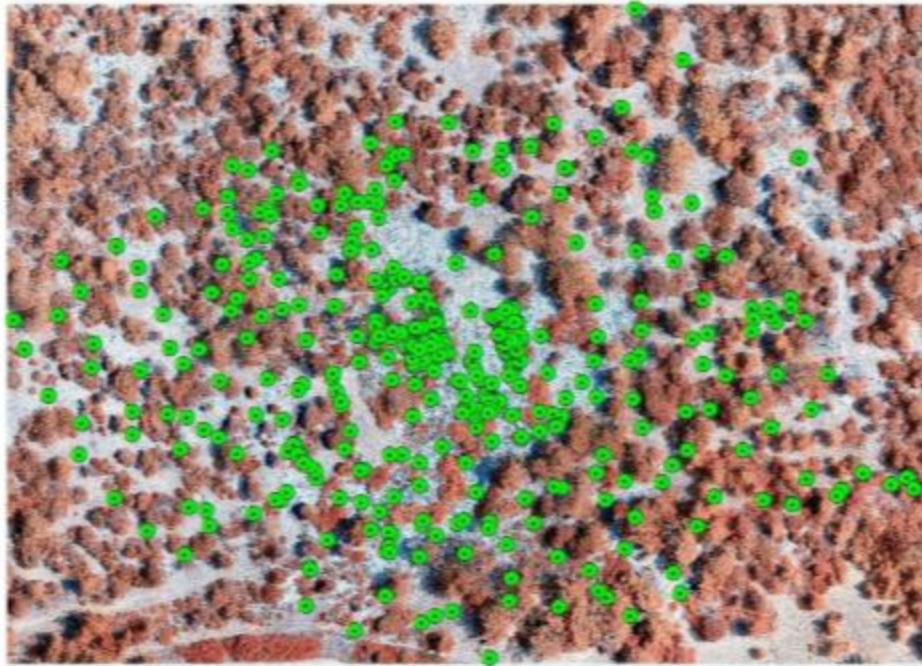


Figure 11. Test Site A -NIR orthophotomosaic with reference points



Figure 12. Ground photos of Test Site B- Vasiliko area, Cyprus, Greece

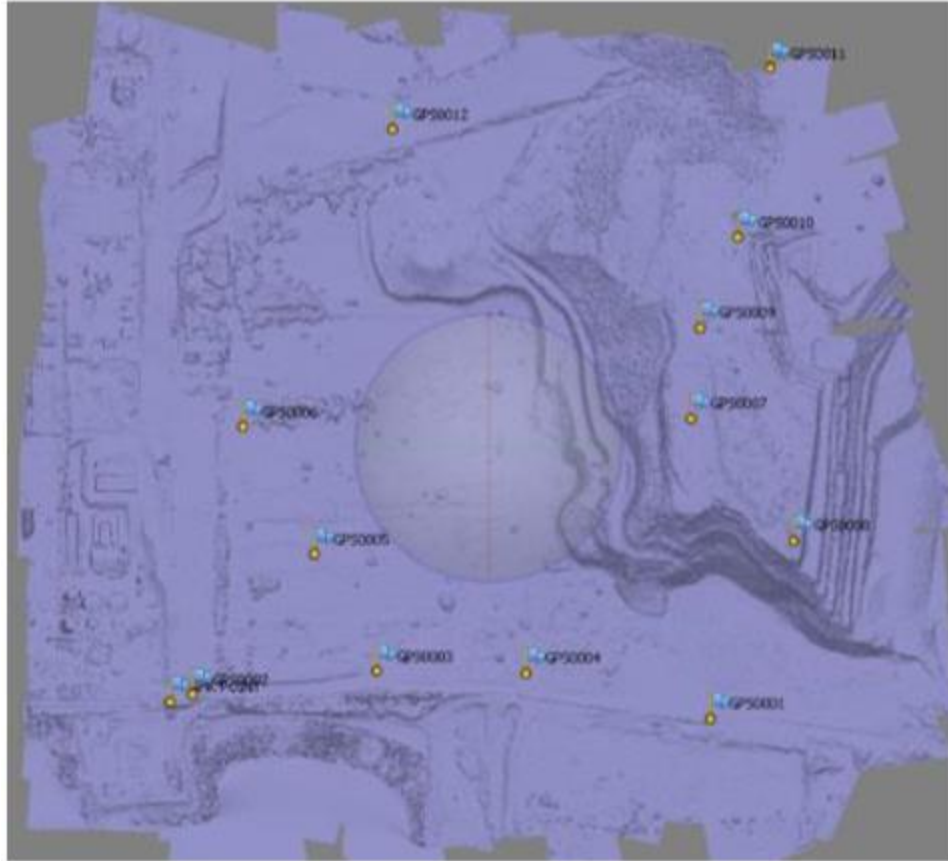


Figure 13. Ground photos of Test Site B



Figure 14. Test Site b NIR orthophotomosaic with reference points (left) and Test Site B orthophotomosaic, with 1 m contours (right)

Results

A threshold of 0.09 was chosen and a cubic interpolation was done to Test Site A and a linear interpolation was done to Test Site B.

Table 2. RGB and NIR processing results of Test Sites A and B

	RGB-A	NIR-A	Com-A	RGB-B	NIR-B
No of photos	261	174	442	118	111
Average flying height [m]	78	101	87	178	178
Overlaps	70%	70%	70%	70%	70%
Base [m]	25.30	32.77	28.34	57.75	57.75
Tie points	249547	169821	343420	271256	235332
Reprojection error in tie points [pix]	0.700	0.607	0.842	0.659	0.651
Average GSD [m]	0.022	0.028	0.022	0.056	0.056
Number of GCPs	38			13	
GCP residuals X [m]	0.014	-	0.015	0.048	0.039
GCP residuals Y [m]	0.021	-	0.019	0.026	0.039
GCP residuals Z [m]	0.037	-	0.036	0.080	0.064
Average pixel error in GCP	0.741	-	0.928	0.804	0.138
Average density of DSM points per m ²	-	-	123.9	20.0	20.3

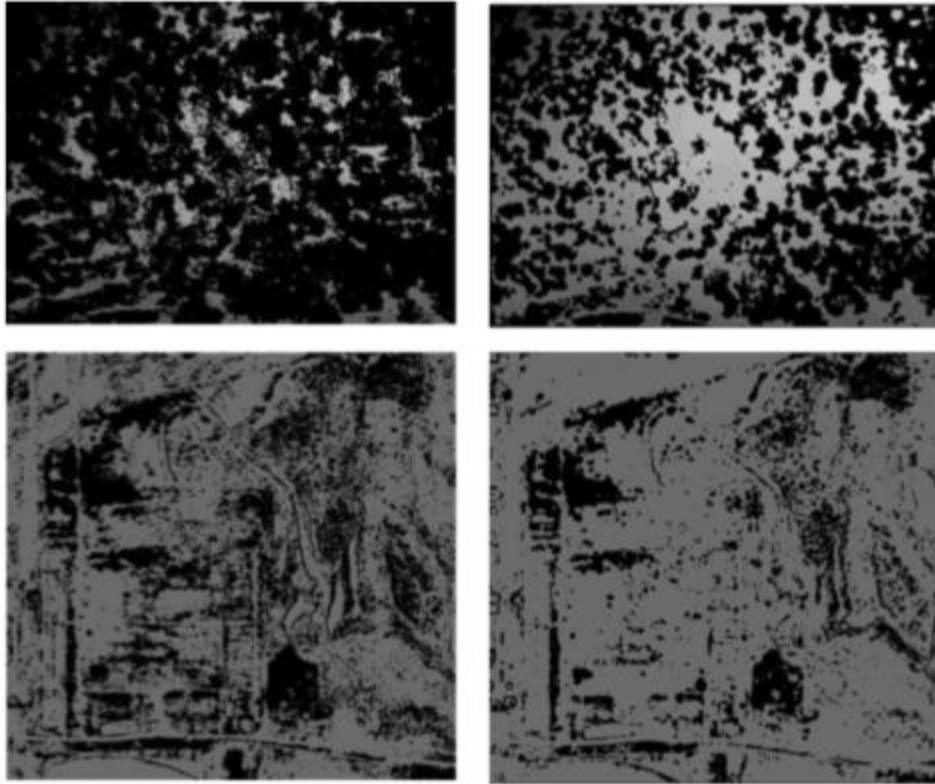


Figure 15. Initial mask with NDVI threshold of 0.09 (left) and after morphological filtering (right for Test Site A (top) and Test Site B (bottom))

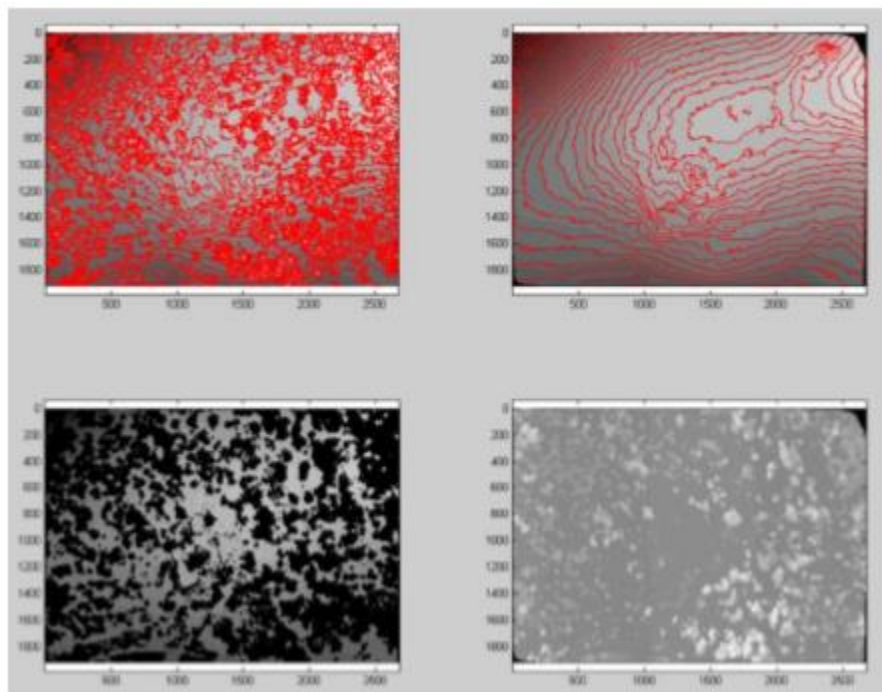


Figure 16. Test Site A; Overlaid contour lines on the initial DSM (top left), mask (bottom left), 1 m contour lines overlaid on the derived DTM (top right), and NDSM (bottom right)

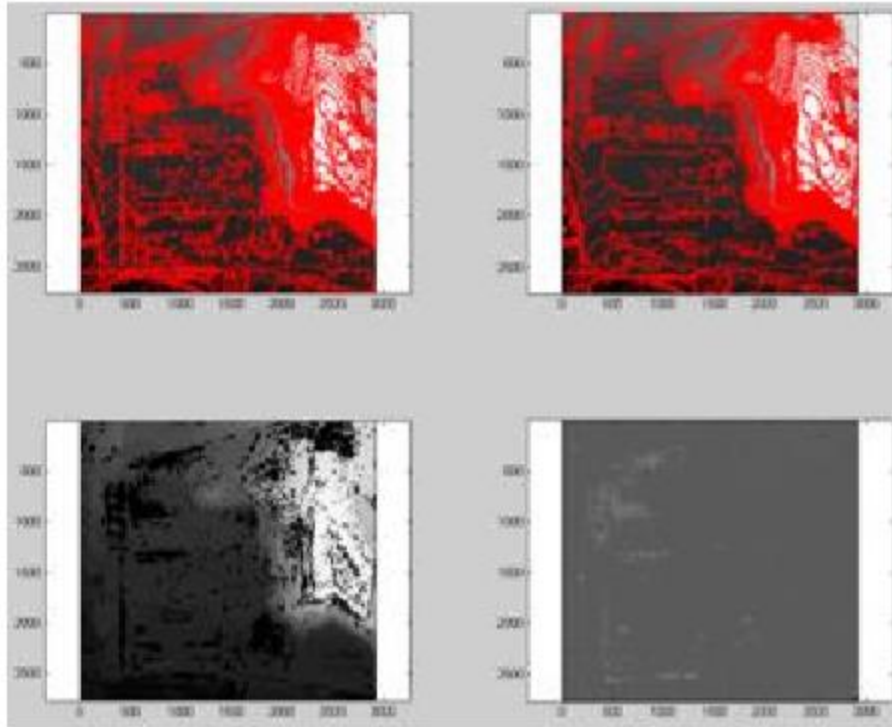


Figure 17. Test Site B; Overlaid contour lines on the initial DSM (top left), mask (bottom left), 1 m contour lines overlaid on the derived DTM (top right), and NDSM (bottom right)

To evaluate accuracy, a large amount of reference points were gathered on areas of vegetation and bare ground. The height precision of a point from an impeccable stereopair is given by:

$$\sigma_z = \frac{H^2}{cB} \sigma_p$$

where

- σ_z , the accuracy of elevation
- H, the flying height above the object
- c, the principle distance
- B, the base of the stereopair
- σ_p , the precision of measuring x – parallax

$$\sigma^2_{f(x,y)} = \left(\frac{\partial f}{\partial x}\right)^2 \sigma^2_x + \left(\frac{\partial f}{\partial y}\right)^2 \sigma^2_y$$

Table 3. Statistics of errors on reference point which are classified as ground or vegetation points based on the NDVI masks created.

	A-on ground points	A-on vegetation points	B-on ground points	B-on vegetation points
DSM				
# of points	316	160	77	60
Mean [m]	-0.123	-0.891	-0.063	-1.388
StdDev [m]	0.194	1.855	0.321	1.638
RMS [m]	0.230	2.051	0.325	2.137
Min [m]	-1.133	-9.239	-1.445	-8.607
Max [m]	0.367	0.456	0.894	1.603
DTM				
# of points	316	160	77	60
Mean [m]	-0.123	-0.029	-0.063	-0.064
StdDev [m]	0.194	0.405	0.321	0.524
RMS [m]	0.229	0.405	0.325	0.524
Min [m]	-1.133	-1.027	-1.445	-1.301
Max [m]	0.367	1.304	0.894	1.722

Conclusions

The study concluded that incorporation of NIR imagery to eliminate vegetation from a DSM can increase the DTM's accuracy. This method can produce DTMs that describe the terrain well enough to act as an alternative option when LiDAR is not available. The quality of results depends on various factors such as morphology, density, area covered by vegetation, the NDVI threshold, and the interpolation method used.

COMPARISON OF THE PERFORMANCES OF GROUND FILTERING ALGORITHMS AND DTM GENERATION FROM A UAV-BASED POINT CLOUD

Serifoglu Yilmaz, C., & Gungor, O. (2018). Comparison of the performances of ground filtering algorithms and DTM generation from a UAV-based point cloud. Geocarto international, 33(5), 522-537.

Compared to LiDAR technology, Unmanned Aerial Vehicles (UAVs) are much less costly and easier to use. This study evaluated five widely used ground filtering algorithms: Progressive Morphological (PM) 1D/2D, Maximum Local Slope (MLS), Elevation Threshold with Expand Window, and Adaptive TIN. This study used ALDPAT v.1.0 software to test the algorithms.

Progressive Morphological 1D/2D Algorithm

PM uses an elevation difference threshold and a window whose size increases gradually to remove points belonging to above ground objects with different sizes. The algorithm generates a regularly spaced minimum surface grid by using the minimum elevation values in each cell. If a grid does not have elevation values then the elevation of the closest point will be assigned. The

PM algorithm uses dilation and erosion operations. The first operation is performed successively as the window size increases gradually. The window can either be one-dimensional (PM1D) or two dimensional (PM2D). $dh_{P,k}$ is the elevation difference between the original and filtered surface at point P in the kth iteration, and $dh_{T,k}$ is the elevation difference threshold. In each kth opening operation, if $dh_{P,k} \leq dh_{T,k}$ then the point is labelled as a ground point. The iterations continue until the size of the window is greater than a predefined maximum value, which is chosen slightly greater than the size of the largest above-ground object.

MLS Algorithm

The MLS algorithm identifies ground points by comparing the local slope between each LiDAR point and neighboring points. This algorithm overlaps LiDAR points with a regularly spaced grid network where each grid represents the elevation of the LiDAR points. Each point $p_j(x_j, y_j, z_j)$ is assigned to each grid with respect to x and y coordinates. If more than one point falls into the grid, then the elevation of the grid is set to the elevation of the point with the minimum elevation is identified. The ground point, $p_0(x_0, y_0, z_0)$, is identified if the maximum slope, $s_{0,max}$, between point p_0 and points within a predefined radius is smaller than a predefined maximum slope threshold.

Parameter	MLS			
	Raw	Low density	Medium density	High density
Cell size	0.4	0.4	0.5	0.5
Maximum slope	0.7	0.7	0.7	0.7
Minimum distance	0.3	0.2	0.1	0.08
Search radius	40	40	40	40

Figure 18. MLS algorithm parameters

ETEW Algorithm

The ETEW algorithm classifies ground and non-ground points by using a search window whose size gradually increases. Firstly, the data is divided into square grid cells and all points except for the ones with minimum elevations are removed. The grid size is increased in the next iteration and a minimum elevation is defined. The elevation differences between the lowest point and the other points are calculated and any points higher than the predefined elevation threshold are removed. The algorithm increases the grid size and threshold values with each iteration until there are no more points to remove. Let $Z_{i,j}$ be the elevation value of point $p_{i,j}$ in the j th grid in the i th iteration, $Z_{i,j,min}$ be the minimum elevation value in the grid, and $h_{i,T}$ be the elevation difference threshold. If $Z_{i,j} - Z_{i,j,min} > h_{i,T}$ then point $p_{i,j}$ is removed in the i th iteration.

Parameter	ETEWE			
	Raw	Low density	Medium density	High density
Cell size	0.4	0.4	0.3	0.3
Slope	0.4	0.4	0.5	0.5
Iteration number	6	6	8	8

Figure 19. ETEW algorithm parameters

ATIN algorithm

The ATIN algorithm uses the distance between each point and generated TIN surface to identify ground points by firstly dividing the data into square grids. The seed points, points with minimum elevations in initial ground data, are then chosen for each grid and used to generate the reference TIN surface. Candidate points, unclassified ground points, are added to each of the triangles in the TIN and classified by using the distance between the candidate point and triangular surface and the angle between the candidate point and vertices of the triangle. Candidate points are classified as ground points if the calculated distance and angle are smaller than predefined thresholds. This process continues until all points are classified.

Parameter	ATIN			
	Raw	Low density	Medium density	High density
Cell size	0.5	0.3	0.1	0.2
Z-difference	0.18	0.18	0.1	0.1
Initial grid size	20	20	20	20
Angle threshold	5	5	5	5
Tile x-y width	20	20	20	20

Figure 20. ATIN algorithm parameters

Accuracy assessment of the filtered point clouds

There are two types of error in the process: omission and commission. Omission error occurs when there is incorrect removal of the ground points and commission error is where non-ground points are classified as ground points. To evaluate the ground filtering process, randomly select test points. These points and all points whose distances to the selected test points are smaller than a predefined threshold are also selected as test points. One hundred test points were selected from each point cloud (i.e. the raw, low-density, medium-density and high-density point clouds). To acquire the same amount of test points for all densities, a radius threshold of 3, 1, 0.5, and 0.15 m for the raw, low-density, medium-density, and high-density data, respectively was used. As a result, 688, 662, 637 and 700 test points were chosen for the raw, low-density, medium-density and high-density data, respectively. The metric used to assess accuracy are type I, type II, and total error which are given as:

$$\begin{aligned} \text{type I error} &= \frac{a}{GP} \\ \text{type II error} &= \frac{b}{NGP} \\ \text{Total error} &= \frac{a + b}{GP + NGP} \end{aligned}$$

where a is the number of the ground points classified as non-ground (omission), b is the number of the non-ground points classified as ground (commission), GP is the total number of the ground points, and NGP is the total number of non-ground points.

The McNemar test was also used to evaluate accuracy of the filtering algorithms. The McNemar test calculates the chi-squared value between two data sets. The difference of the two datasets is significant if the calculated chi-squared value is greater than the critical value.

DTM generation

Ordinary Kriging (OK) algorithm was used to interpolate the DTM of the study area. Interpolation was conducted using script written in MATLAB. The resolution of the DTM was estimated by:

$$S = \sqrt{\frac{A}{n}}$$

where n is the total number of points and A is the total area.

Study area and data preparation

The study area is the Karadeniz Technical University (KTU) campus in the city of Trabzon, Turkey. The area's dimensions are 178 m x 410 m, which includes buildings and trees.

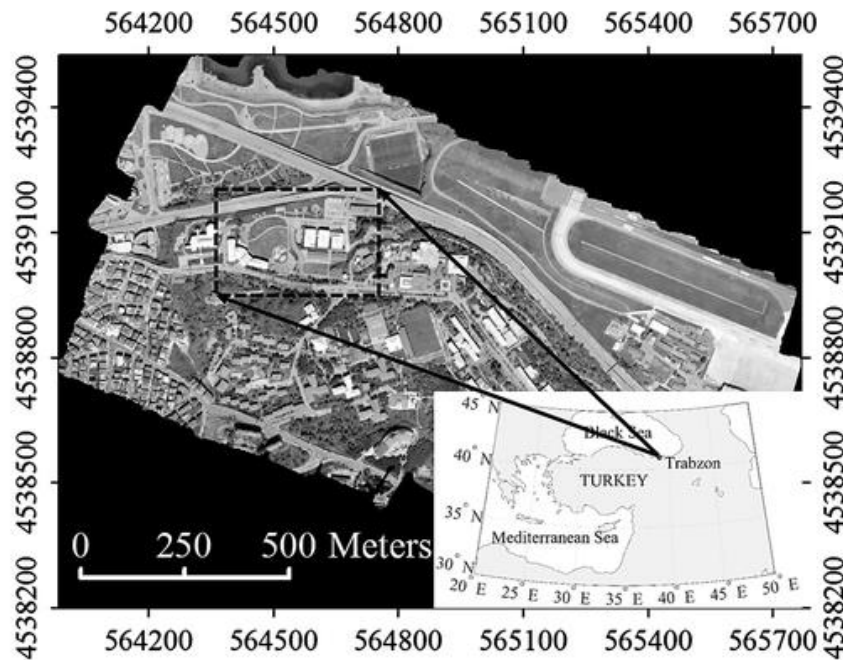


Figure 21. Study area in Trabzon, Turkey

Image size	3648 × 2736
Focal length	6.0 mm
ISO sensitivity	AUTO, ISO80 – 3200
Image sensor	1/1.7 inch
F-aperture	F1.9 – F9
Weight	219 g

Figure 22. Specifications of the RICOH GR DIGITAL IV digital camera

Before the flight, 12 ground control points (GCPs) were established and distributed evenly throughout the campus for georeferencing. A RICOH GR DIGITAL IV digital camera, the standard camera of the Gatewing X100 UAV, was used to capture images from an altitude of 185 m. The 410 minute flight was conducted along 9 oaths and 256 aerial photos were captured. The resolution of each aerial photo was 7 cm. Agisoft Photoscan Professional software was used to process the aerial photos where key points are extracted phot by photo. After the GCPs are used to georeference the point cloud obtained with image matching and calculate 3D coordinates of the key points with automatic aerial triangulation. After, the raw point cloud with a density of 0.1 point/m² was generated. Agisoft Photoscan offers five density choices as lowest, low, medium, high and highest. In this study, low, medium, and high-density point clouds were generated. The software can also calculate depth information for each camera and combines them into a single, dense point cloud based on the estimated camera positions. The densities of the low-density, medium-density, and high-density point clouds are 4.2, 16.5, and 61.1 point/m², respectively. Finally, a 25 cm orthophoto image was produced for the study area.

Results

The accuracy of the filtering results was tested quantitatively and qualitatively. Qualitatively, results were analyzed visually and was done by overlapping the filtered point cloud with the produced high resolution orthophoto image. Quantitatively, the test points were selected randomly from the unfiltered point cloud of each of the raw, low-density, medium-density and high-density data. Then, the filtered point cloud, test points, and orthophoto were overlapped to visually evaluate whether the test points were removed.

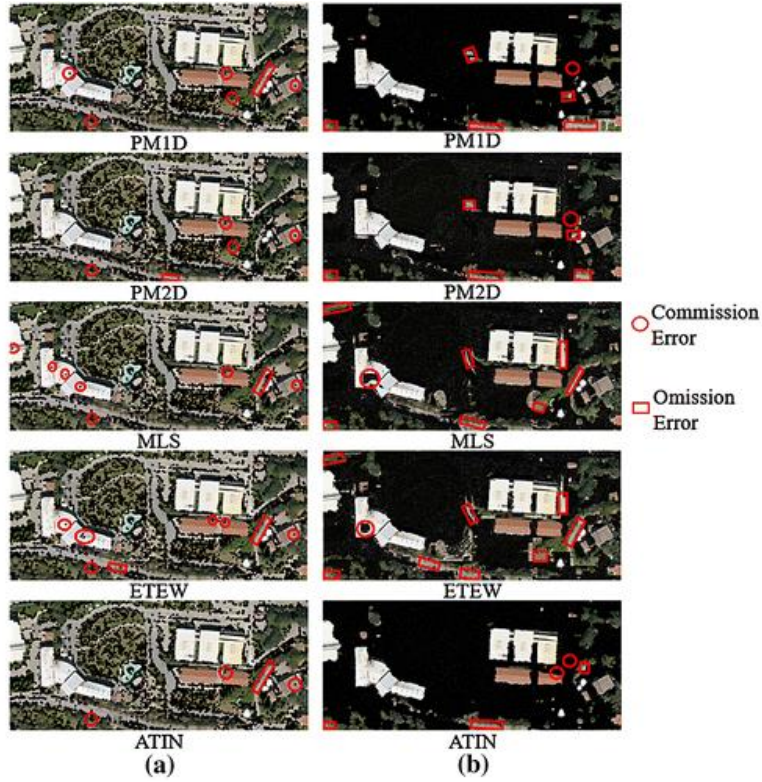


Figure 23. (a) Filtering results of the raw data, (b) filtering results of the low-density data

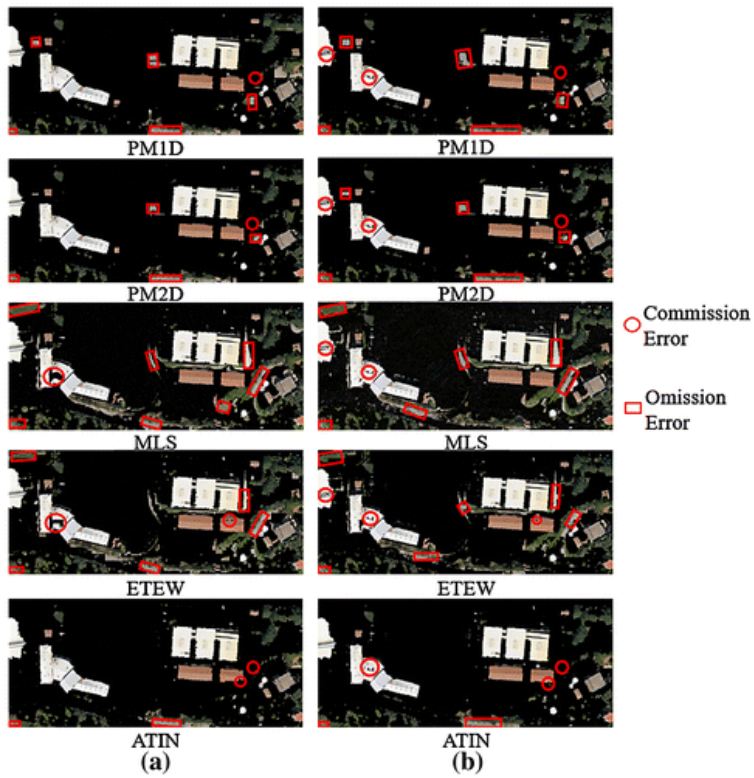


Figure 24. Filtering results of the medium-density data, (b) filtering results of the high-density data

Data-set	Filtering algorithm	Type I error (%)	Type II error (%)	Total error (%)	Chi-squared values
Raw data	PM1D	9.70	11.30	10.00	325.26
	PM2D	1.90	28.00	5.90	395.01
	MLS	11.30	10.40	11.20	306.11
	ETEW	11.80	13.20	12.10	280.50
	ATIN	5.10	12.30	6.20	415.91
Low-density data	PM1D	19.42	18.20	19.03	233.40
	PM2D	18.32	12.00	16.50	284.81
	MLS	33.30	6.70	23.40	205.84
	ETEW	38.00	9.10	29.10	159.01
	ATIN	18.50	15.80	17.60	258.19
Medium-density data	PM1D	30.40	7.90	23.20	210.30
	PM2D	28.10	9.30	22.10	216.36
	MLS	69.35	8.90	50.08	36.20
	ETEW	64.10	2.50	44.50	81.96
	ATIN	30.00	4.40	21.90	237.86
High-density data	PM1D	51.20	10.60	40.20	84.35
	PM2D	49.20	10.60	38.80	92.07
	MLS	70.80	6.30	53.40	40.06
	ETEW	69.30	6.40	52.30	44.28
	ATIN	44.30	6.40	34.00	136.52

Figure 25. Calculated Type I error, type II error, and chi-squared values

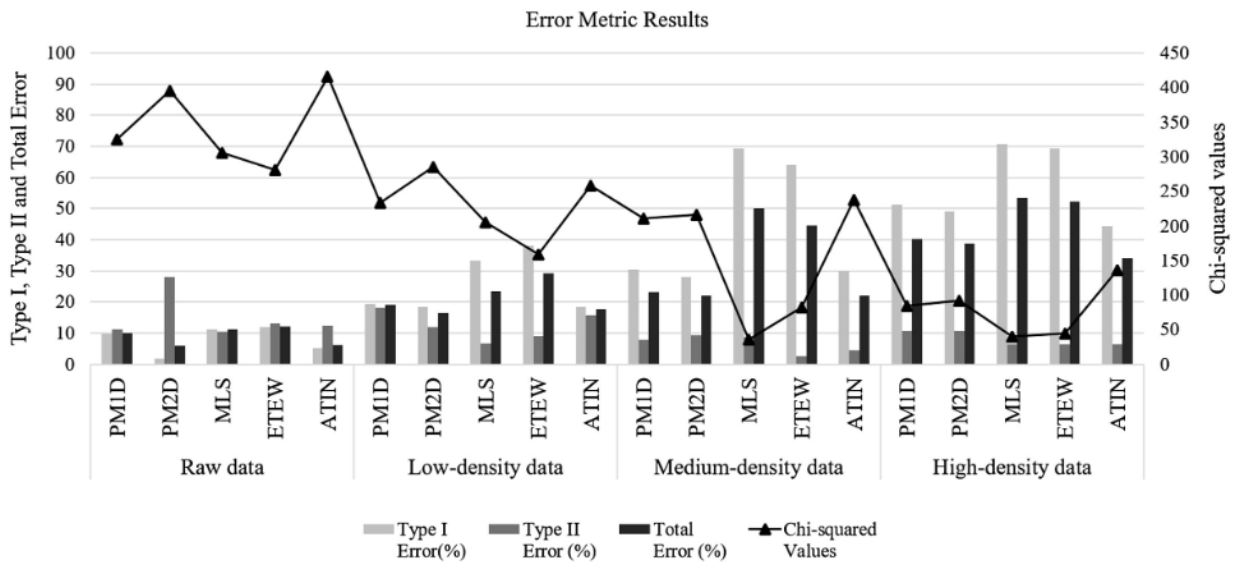


Figure 26. Graph of calculated type I error, type II error, and chi-squared values

The MLS algorithm was found to be the one most affected by increase in point density but had the worst performance when filtering medium-density and high-density data. It is better to use the MLS algorithm to filter the sparse point clouds. The PM2D algorithm performed better than the PM1D algorithm, but the performances of the algorithms are close as the point density increases. Considering the total error and chi-squared values, the ATIN algorithm was found to be the most accurate and can be used to filter the point clouds with high densities.

Because the ATIN algorithm was found to be the most successful algorithm, the ATIN result was used to interpolate the DTM. The filtered point cloud contained 1,284,763 points and the study area covered 72,980 m² which resulted in a spatial resolution of 25 cm for the DTM.

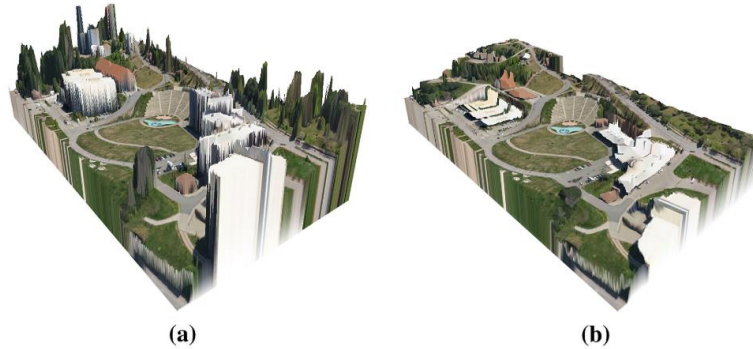


Figure 27. Orthophoto image draped over the produced (a) DSM and (b) DTM.

To test the accuracy of the produced DTM, test points were established within the study area. A total of 87 test points were established for flat areas (test site 1), 163 test points for sloping areas (test site 2), and 128 test points for areas close to above ground objects (test site 3). The Real Time Kinematik (RTK) GPS technique was used to measure positions of all test points. Root Mean Square Error (RMSE), Standard Deviation of Residuals (SDR), Mean Absolute Error (MAE), and Mean Error (ME) were calculated for each test site by using the measured elevation of the test points and their corresponding elevations on the DTM. The mathematical equations for RMSE, MAE, ME, and SDR are given as:

$$\begin{aligned}
 \text{RMSE} &= \sqrt{\frac{1}{n} \sum_{i=1}^n (M_z(x, y) - \text{DTM}_z(x, y))^2} \\
 \text{MAE} &= \frac{1}{n} \sum_{i=1}^n (|M_z(x, y) - \text{DTM}_z(x, y)|) \\
 \text{ME} &= \frac{1}{n} \sum_{i=1}^n (M_z(x, y) - \text{DTM}_z(x, y)) \\
 \text{SDR} &= \sqrt{\frac{\sum_{i=1}^n (R_i - \bar{R})^2}{n - 1}} \quad (3)
 \end{aligned}$$

METHODOLOGIES FOR VEGETATION IDENTIFICATION FROM UNMANNED AERIAL VEHICLES (UAV)-BASED PHOTOGRAMMETRIC DIGITAL SURFACE MODEL USING MACHINE LEARNING

UAVs AND MACHINE LEARNING REVOLUTIONISING INVASIVE GRASS AND VEGETATION SURVEYS IN REMOTE ARID LANDS

Sandino, J., Gonzalez, F., Mengersen, K., & Gaston, K. J. (2018). UAVs and machine learning revolutionizing invasive grass and vegetation surveys in remote arid lands. Sensors, 18(2), 605.

The goal of this study was to delineate a process to detect and create a pixel-wise segmentation of invasive grasses in Cape Range National Park, Australia. It involved the use of unmanned aerial vehicles (UAVs) equipped with high-resolution RGB cameras and a data processing approach using machine learning algorithms.

Methodology

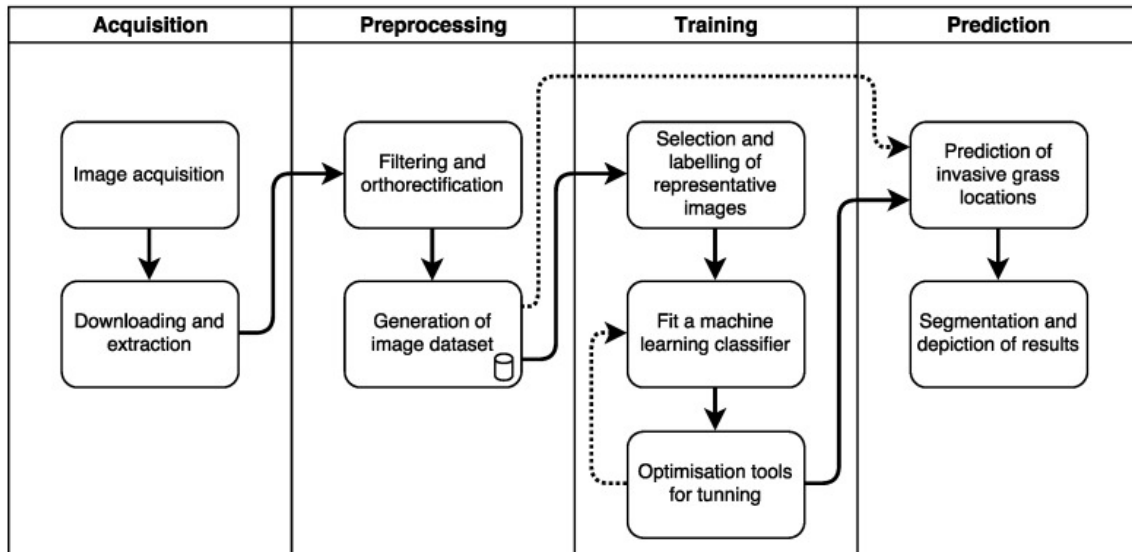


Figure 28. Process Flowchart

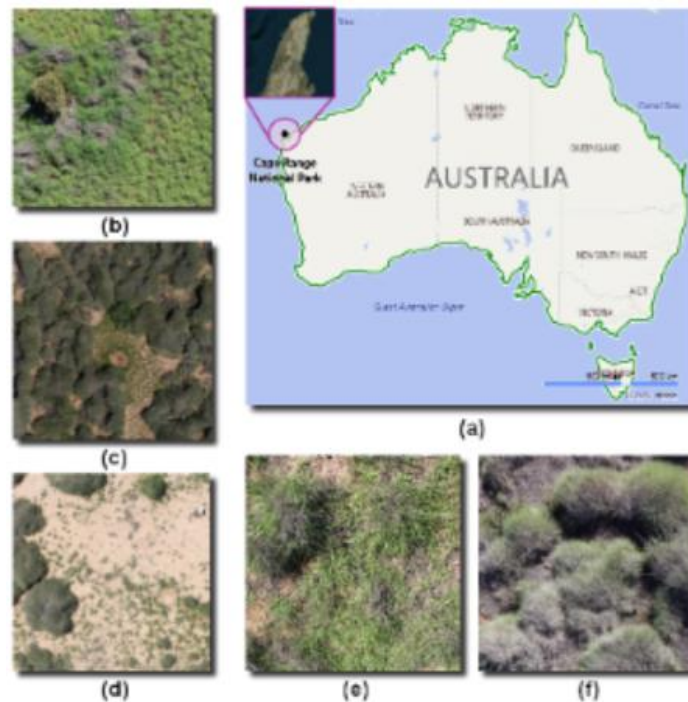


Figure 29. (a) Geographical Location with Cape Range National Park highlighted, (b) Aerial view of high density of buffel grass, (c) Area with high density of spinifex, (d) Area with low density of invasive grasses, (e) Buffed grass, (f) Spinifex

Data Acquisition

A Canon EOS 5DsR digital camera with a 50.6 MP camera, 28 mm focal length, ISO-400 speed, a full frame complementary metal oxide semiconductor (CMOS) sensor of 36 mm X 24 mm, a 625 μ s exposure time, and a GPS sensor was used and mounted on a DJI S800 EVO Hexa-rotor UAV. Over 500 images were collected and filtered and orthorectified on Agisoft Photoscan 1.2. The orthomosaic image was of 44,800 x 17,200 which was a huge size and because of this, it was split into 4,816 items of 400 x 400 pixels in Tagged Image File (TIF) and Keyhole Markup Language (KML) formats. Representative samples in cropped regions were classified using HNU Image Manipulation Program (GIMP) 2.8.22 to fit the classifier. The generated images were then processed with Python 2.1.17 and third party libraries for data manipulation machine learning, including eXtreme Gradient Boosting (XGBoost) 0.6, Scikit-learn 0.19.1, OpenCV 3.3.0, and Matplotlib 2.1.0.

Because the invasive grasses are found in a variety of regions, 10 images were carefully selected and evaluated through visual interpretation. Invasive grasses and other common vegetation were highlighted using the “Bucket fill” tool in the GIMP software. To label the images, a mask was created by assigning integer values to each highlighted pixel. Each bright colored pixel was filtered using the following equation:

$$H_{(x,y)} = \begin{cases} a & \text{if } S_{(x,y)} = F_{(R,G,B)} \\ 0 & \text{otherwise} \end{cases}$$

where H is the mask of sample S and a is the integer value for each bright color value F(R,G,B). The values of a are defined as: 1= buffel grass, 2=soil and road, 3= bushes, 4= shadow, 5= dry vegetation, and 6= spinifex.

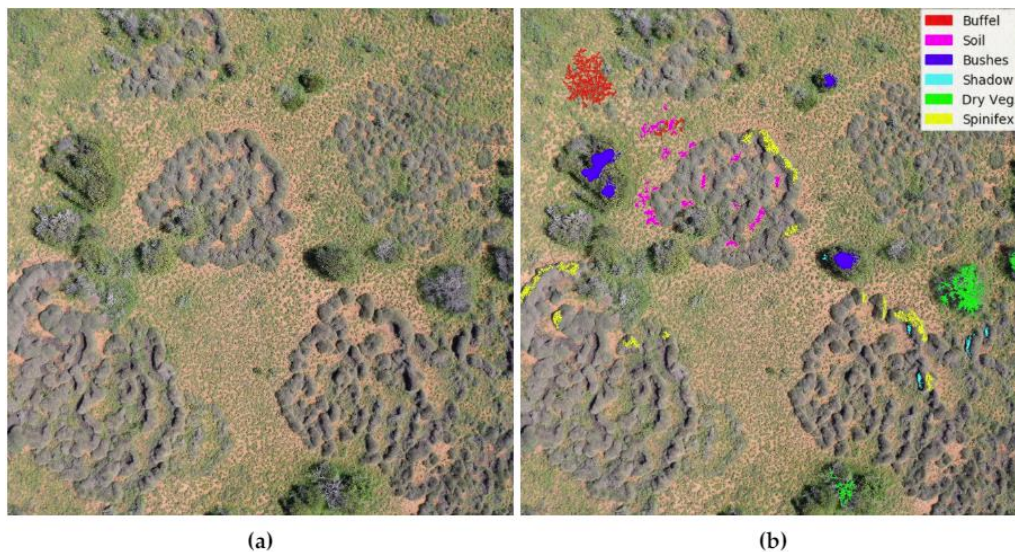


Figure 30. Image labelling examples (a) Representative sample (b) Highlighted regions with bright colors

Classification Algorithm

Algorithm 1 Detection and segmentation of invasive grasses using high-resolution RGB images.

Required: orthorectified image set I . Representative samples set G . Sample masks set H
Training

- 1: **for** $i \leftarrow 1, n$ **do** $\triangleright n = \text{total images in } G \text{ (labelled data)}$
- 2: Load G_i and H_i images
- 3: Convert colour space of G_i into HSV
- 4: Insert each colour channel into a feature array D
- 5: Use 2D filters on G_i and insert their outputs into D
- 6: From G_i and H_i , filter only the pixels with assigned labelling on D
- 7: **end for**
- 8: Split D into training data D_T and testing data D_E
- 9: Create a XGBoost classifier X and fit it using D_T
- 10: Use K -fold cross validation with D_E $\triangleright \text{number of folds} = 10$
- 11: Perform grid search to tune X parameters

Prediction

- 12: **for** $i \leftarrow 1, m$ **do** $\triangleright m = \text{total images in } I$
 - 13: Load I_i image
 - 14: Convert colour space of I_i into HSV
 - 15: Scan every pixel and predict the object using X
 - 16: $O_i \leftarrow$ Convert the data into a 2D image
 - 17: Export O_i into TIF format
 - 18: **end for**
 - 19: **return** O_i
-

Figure 31. Classification Algorithm

The algorithm identifies and filters the highlighted regions, trains a gradient boosted decision tree classifier, cross validates the classification rates, predicts unlabeled data, and displays results. The processing stage of the algorithm transforms the read data into a selection of features or attributes, which are consequently processed by the classifier. To get the feature array D , representative sample images, G , are first converted from the default RGB to the hue, saturation, value (HSV) color model. Next, filters are applied on G and the outputs are inserted into D . The 2D filters are then used to calculate the variance into a subset of pixel neighbors in a window using the following equations:

$$X = \frac{1}{w^2} \begin{bmatrix} 1 & 1 & \dots & 1 \\ 1 & 1 & \dots & 1 \\ \vdots & \vdots & \ddots & \vdots \\ 1 & 1 & \dots & 1 \end{bmatrix}$$

$$s^2 = E[X^2] - E[X]^2$$

where X is the kernel of the filter to estimate the mean value of the processed image, w is the window size, and s^2 is the variance defined as the subtraction between the estimation of mean of square and the square of the mean. The array of the features D has 10 items: hue, saturation, value, variance filters where w is 3 and 15, variance filters on saturation where w is 3 and 1, and

variance filters of the grayscale image from G_i where w is 3, 7, and 15. Next, previously labeled pixel locations are filtered with masks, H , using the equation:

$$D_j = \begin{cases} [G_i(x, y), H_i(x, y)] & \text{if } H_i(x, y) \neq 0 \\ \text{null} & \text{otherwise} \end{cases}$$

where D_j is the 2d output array of the operation, $G_i(x,y)$ is the sample image, and $H_i(x,y)$ is the labelled counterpart of G_i at position (x,y) . In total, over 300,000 pixel wise samples were filtered and split randomly into a training and testing data array. Step nine of the algorithm consists of processing data into the XGBoost classifier that is optimized for large tree structures, high execution speed, and excellent performance. Step 11 consists of running a grid search method to estimate the hyper parameters for this classifier like the number of estimators, the learning rate, and the maximum depth and the grid search method returns the optimal combination. The optimal hyper- parameter values for this study were: estimators=100, learning rate =0.1, and maximum depth = 3. The estimators are the number of trees, the learning rate is the step size of each boosting step, and the maximum depth is the maximum depth per tree that defined the complexity of the model. Finally, the orthorectified images are processed in a loop using the trained classifier and the same data conversion considerations that were applied on the training section and the classified pixels are identified in distinguishable colors and exported as TIF.

Results

Table 4. eXtreme Gradient Boosting (XGBoost) classifier confusion matrix

	Predicted	Buffel	Soil	Bushes	Shadow	Dry vegetation	Spinifex
Labelled	Buffel	25,256	17	156	0	4	362
	Soil	15	25,196	1	0	1	0
	Bushes	632	1	3913	2	21	81
	Shadow	0	1	0	7729	0	0
	Dry vegetation	8	10	6	2	5734	159
	Spinifex	508	2	20	0	171	15,649

Table 5. Classification report from confusion matrix of Table 1

Class	Precision (%)	Recall (%)	F-Score (%)	Support
Buffel	95.60	97.91	96.75	25,795
Soil	99.88	99.93	99.90	25,213
Bushes	95.53	84.15	89.84	4650
Shadow	99.95	99.99	99.97	7730
Dry vegetation	96.68	96.87	96.78	5919
Spinifex	96.30	95.71	96.00	16,350
Mean	97.32	95.76	96.54	$\Sigma = 85,657$

Literature Review of Methodologies for Vegetation Identification and Removal

From Table 5, precision is defined by the ratio of true positives and the sum of true positives and false positives, recall is the ratio between true positives and the sum of true positives and false negatives, F-score is the mean of precision and recall, and support is the number of tested pixels per class.

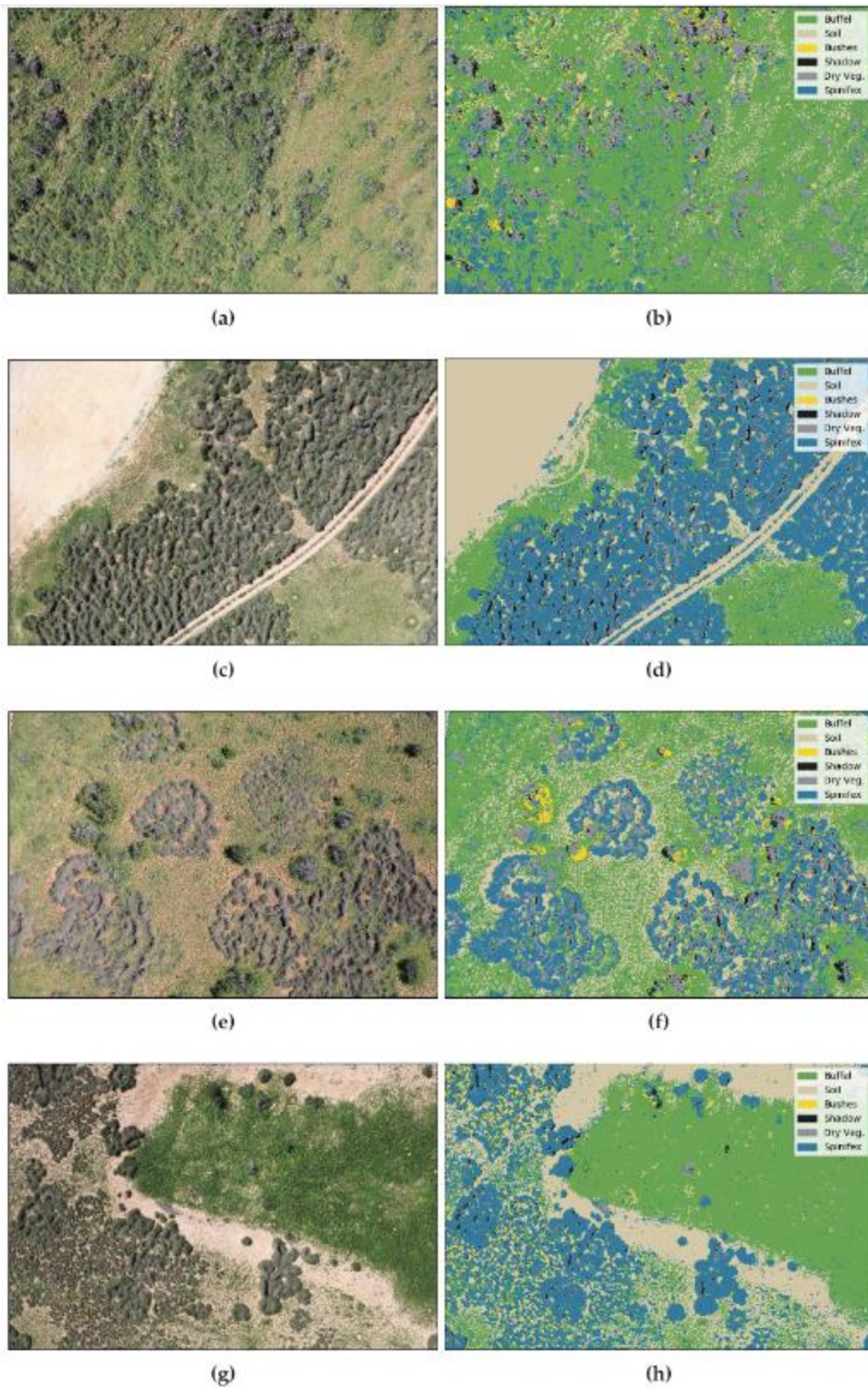


Figure 32. Pixel-wise segmentation from RGB color model images using Algorithm 1 (a,c,e,g). Orthorectified RGB images with predicted classes (b, d, f, h).

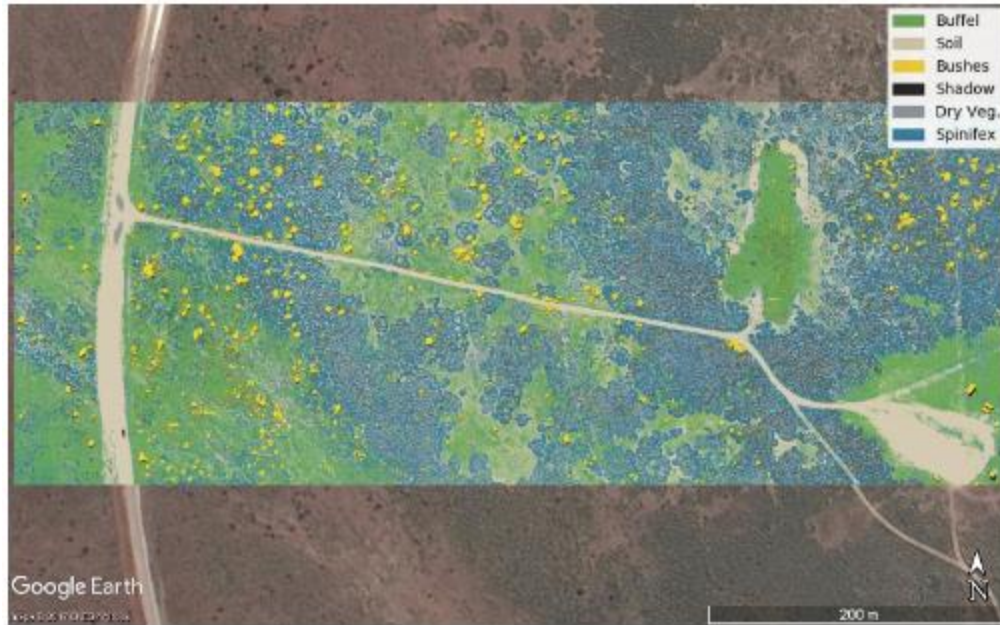


Figure 33. Predication of invasive grasses in Cape Range National Park displayed on Google Earth.

Conclusions

The accuracy and segmentation indicators served to validate the methodology to map vegetation. Any observed misclassification of buffel and spinifex were the result of human error when the sample data was first labeled. The proposed methodology showed detection rates of 96.75% and 96% for single mapping of buffel grass and spinifex, respectively, and a multiclass detection rate of 96.54%. Invasive grasses were accurately detected at different spatial concentrations with a GSD of 1.015 cm per pixel. Moving forward, work will be focused on implementing unsupervised and supervised methods for labeling vegetation to reduce processing times.

MULTI-FEATURE MACHINE LEARNING MODEL FOR AUTOMATIC SEGMENTATION OF GREEN FRACTIONAL VEGETATION COVER FOR HIGH-THROUGHPUT FIELD PHENOTYPING

Sadeghi-Tehran, P., Virlet, N., Sabermanesh, K., & Hawkesford, M. J. (2017). Multi-feature machine learning model for automatic segmentation of green fractional vegetation cover for high-throughput field phenotyping. Plant methods, 13(1), 103.

Accurate vegetation segmentation from the background in digital images is a fundamental and challenging task in phenotyping. Digital RGB cameras are most commonly used for field phenotyping because they are affordable and portable in size. This study proposed a multi-feature learning method to quantify vegetation growth. The proposed method was then compared with other state of the art methods with the following criteria: (1) comparison with ground-truth

images, (2) variation along a day with changes in ambient lighting, (3) comparison with manual measurements, (4) an estimation of performance along the full life cycle of a wheat canopy.

Methodology

The proposed machine learning method involved the acquisition of digital images in time series, extraction of multi-feature color transformation, a supervised classification model to label pixels as foreground or background, and noise reduction using median filtering.

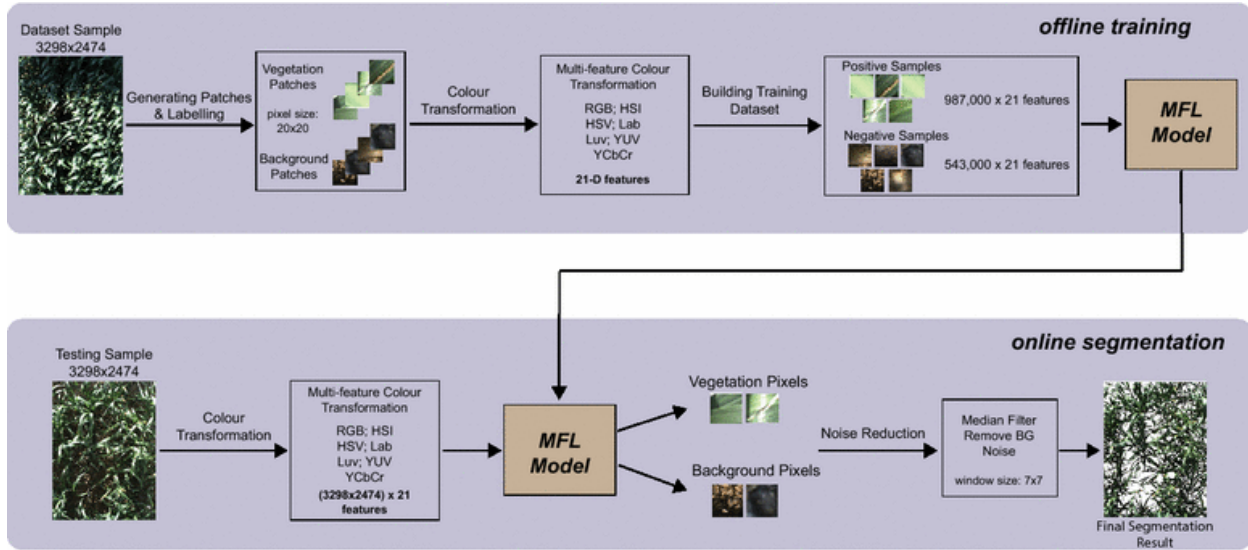


Figure 34. Schematic diagram of proposed methodology

OBJECT-BASED VEGETATION MAPPING IN THE KISSIMMEE RIVER WATERSHED USING HYMAP DATA AND MACHINE LEARNING TECHNIQUES

Zhang, C., & Xie, Z. (2013). *Object-based vegetation mapping in the Kissimmee River watershed using HyMap data and machine learning techniques*. *Wetlands*, 33(2), 233-244.

This study, based on the Kissimmee River watershed, evaluated the applicability of fine spatial resolution hyperspectral data collected from the HyMap sensor for both the community and species level vegetation mapping. Vegetation maps were produced using machine learning methods, Support Vector Machines (SVM) and Random Forest (RF), object based image analysis techniques, and Minimum Noise Fraction (MNF) data transformation.

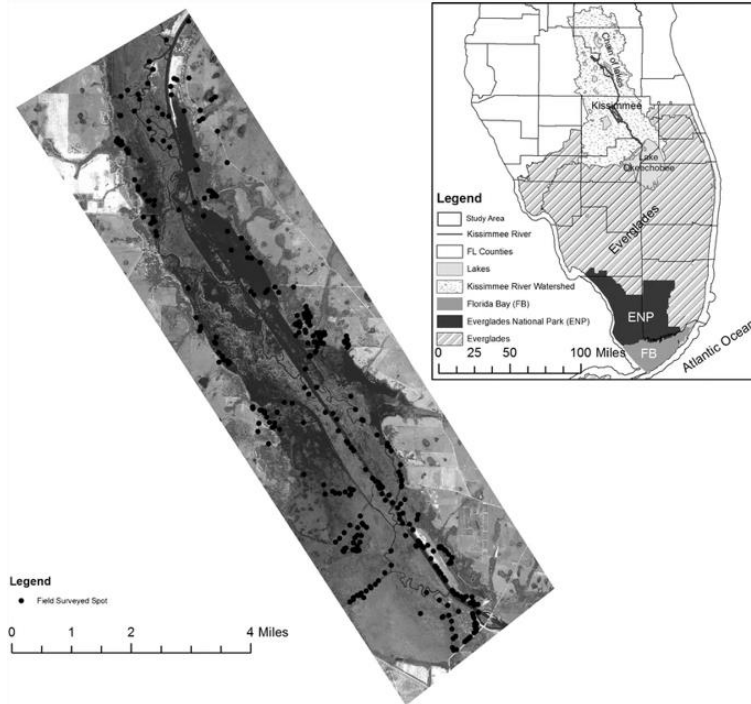


Figure 35. Map of the Greater Everglades, Kissimmee River watershed, study area, and field sampling locations.

The South Florida Water Management District (SFWMD) provided the hyperspectral data and field data for the study. The SVM machine learning method is a non-parametric supervised learning classifier where the goal is to find a hyperplane that can separate the input dataset into a discrete predefined number of classes in a manner similar to the training samples. There are Kernel based SVMs that are used for remote sensing image classification where the radial basis function (RBF) kernel and the polynomial kernel are most commonly used. The RBF has a specified kernel width (γ) while the polynomial kernel has a specified degree (p) and both require a penalty parameter (C) which controls the degree specification. After using a grid search method to define the most optimal parameters, the study used the polynomial kernel with $p=2$ and $C=2$.

The other classification method was a RF decision tree ensemble classifier. The study defines decision trees to split training samples into smaller subdivisions at “nodes” based on decision rules. At each node, tests are performed on the training data to find the most useful variable values at the split. “The RF consists of a combination of decision trees where each decision tree contributes a single vote for assigning the most frequent class to an input vector” (Zhang, et al, 2013). RF requires two parameters: the number of decision trees to create (k) and the number of randomly selected variable (m) for consideration of the split of each node. The study used $m=10$ and trials discovered that $k=100$ was the most accurate.

The accuracy of the object based vegetation maps was compared using an error matrix and calculating a Kappa statistic. The Kappa statistic serves to describe the proportion of correctly classified validation sample after random agreement is removed. The non-parametric McNemar test was used to evaluate the statistical significance of differences in accuracy between different classifications. A significant statistical difference has a 95% confidence level and a z-score larger than 1.96 which is calculated from the McNemar test.

Results

Table 6. Comparison of classification using original data and MNF transformed data

	Original			MNF		
Community-level						
Classifier	Accuracy	Kappa	Time (s)	Accuracy	Kappa	Time (s)
SVM	83%	0.80	45.7	89%	0.87	0.65
RF	74%	0.70	1.47	90%	0.89	0.55
Pairwise statistical test						
	McNemar Test			McNemar Test		
SVM (Original/MNF)	3.6*			Original (SVM/RF)	4.4*	
RF (Original/MNF)	7.8*			MNF (SVM/RF)	1.3	
Species-level (B-Codes)						
Classifier	Accuracy	Kappa	Time (s)	Accuracy	Kappa	Time (s)
SVM	73%	0.72	472.6	85%	0.85	13.7
RF	36%	0.34	5.6	79%	0.79	1.59
Pairwise statistical test						
	McNemar Test			McNemar Test		
SVM (Original/MNF)	6.0*			Original (SVM/RF)	13.7*	
RF (Original/MNF)	15.2*			MNF (SVM/RF)	3.4*	

SVM support vector machine

RF random forest

Original original hyperspectral data with 119 bands

MNF MNF transformed data with 20 bands

*significant with 95% confidence

Table 7. SVM and RF accuracies with different training sizes

SVM		RF		
Community-level				
Training Size	Accuracy	Kappa	Accuracy	Kappa
20%	77%	0.73	79%	0.74
40%	89%	0.86	88%	0.85
60%	86%	0.84	91%	0.89
80%	93%	0.92	92%	0.90
Species-level (B-Codes)				
Training Size	Accuracy	Kappa	Accuracy	Kappa
20%	60%	0.59	61%	0.60
40%	75%	0.75	73%	0.72
60%	81%	0.80	82%	0.82
80%	87%	0.87	85%	0.84

SVM support vector machine

RF random forest

The MNF transformed data were used in these tests

Table 8. Classification accuracy with different number of classes

SVM		RF		
Community-level (Excluded Classes with Lower Accuracies)				
No. of Classes	Accuracy	Kappa	Accuracy	Kappa
5	93%	0.90	95%	0.93
10	88%	0.86	92%	0.91
Species-level (B-Codes) (Excluded Classes with Lower Accuracies)				
No. of Classes	Accuracy	Kappa	Accuracy	Kappa
10	99%	0.98	97%	0.96
20	95%	0.95	92%	0.91
30	94%	0.94	88%	0.87
40	92%	0.92	86%	0.86

SVM support vector machine

RF random forest

The MNF transformed data were used in these tests

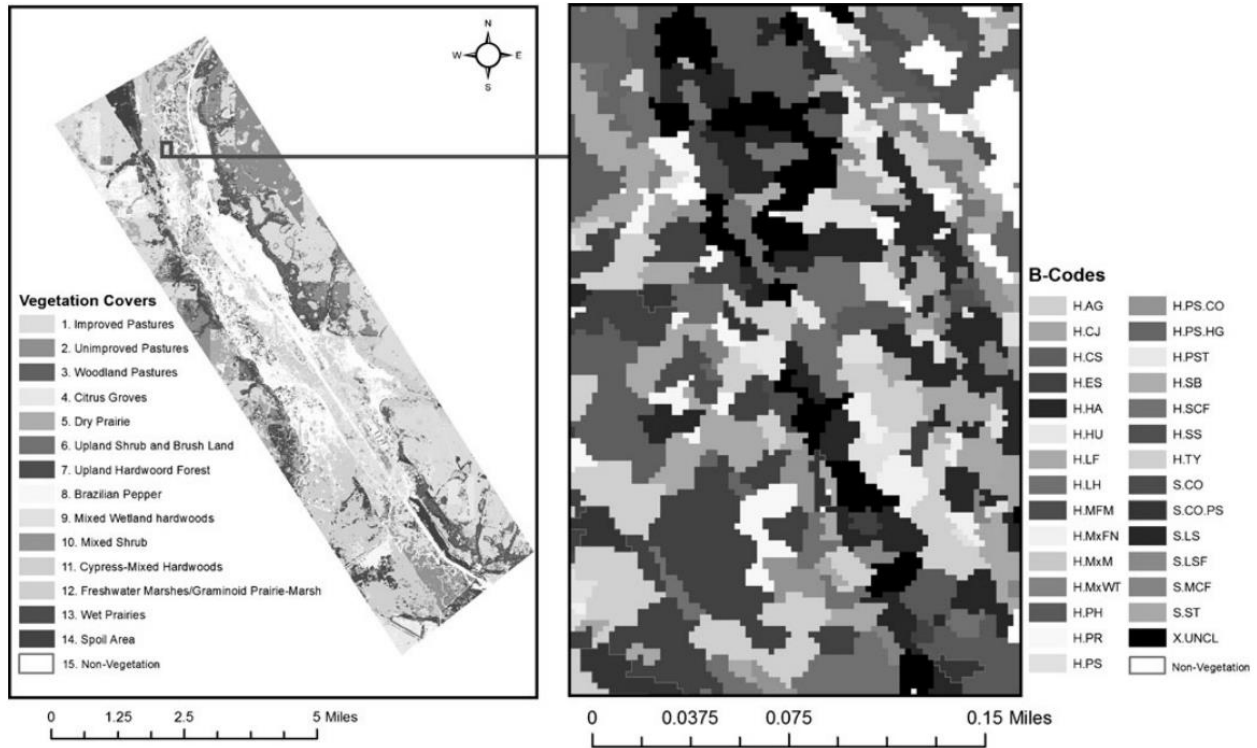


Figure 36. Vegetation community map (left) and vegetation B-Code map (right) from the SVM models.

Table 9. Classification accuracy for each community from SVM and RF classifiers

Community	NR	SVM		RF	
		PA	UA	PA	UA
1. Improved pastures	126	89	85	97	87
2. Unimproved pastures	90	87	83	82	90
3. Woodland pastures	112	93	95	95	96
4. Citrus groves	32	94	94	94	94
5. Dry prairies	20	40	57	30	60
6. Upland shrub and brush land	10	100	100	80	100
7. Upland hardwood forests	34	82	78	94	84
8. Brazilian pepper	34	82	78	94	94
9. Mixed wetland hardwoods	46	83	83	80	82
10. Mixed shrub	42	91	87	81	90
11. Cypress-mixed hardwoods	44	87	86	91	95
12. Freshwater marshes/Graminoid Prairie-Marsh	310	95	96	98	92
13. Wet prairies	54	69	83	67	82
14. Spoil area	32	100	94	100	100
Overall accuracy and Kappa value		Accuracy: 89%		Accuracy: 90%	
		Kappa: 0.87		Kappa: 0.89	

SVM support vector machine
RF random forest
PA Producer's accuracy (%)
UA User's accuracy (%)
NR number of references

Table 10. Classification accuracy for each B-Code from SVM and RF classifiers

B-Code	NFS	SVM		RF		B-Code	NFS	SVM		RF	
		PA	UA	PA	UA			PA	UA	PA	UA
1. H.AF	6	100	90	90	81	29. H.PR	6	100	91	90	71
2. H.AG	5	87	100	87	87	30. H.PS	10	96	83	100	64
3. H.CD	5	71	41	42	100	31. H.PS-CO	6	90	71	63	63
4. H.CJ	5	62	83	25	100	32. H.PS-HG	6	100	90	70	63
5. H.CS	5	100	100	85	85	33. H.PS-PH	6	100	91	81	90
6. H.EC	6	81	90	100	84	34. H.PS-PH-CO	8	92	100	85	80
7. H.EC-PST	4	80	57	100	71	35. H.PST	6	60	42	60	66
8. H.ES	6	90	100	80	100	36. H.RN	6	90	83	72	80
9. H.HA	6	90	100	90	90	37. H.SB	6	100	90	80	72
10. H.HG	6	100	100	100	83	38. H.SCF	6	90	76	72	80
11. H.HU	6	36	80	63	77	39. H.SS	6	100	100	100	83
12. H.JEd	5	100	100	85	100	40. H.TY	7	92	92	85	85
13. H.JEp	5	100	100	100	100	41. S.CO	7	92	92	85	75
14. H.LH	6	80	72	70	77	42. S.CO-PS	6	90	76	81	64
15. H.MFM	6	90	83	63	87	43. S.CO-PS-PH	6	80	66	60	100
16. H.MxE	6	70	100	80	100	44. S.HF	6	100	83	90	69
17. H.MxFA	4	80	66	80	100	45. S.LS	7	57	80	85	85
18. H.MxFN	6	90	100	81	90	46. S.LSF	6	63	77	36	80
19. H.MxM	5	42	100	00	00	47. S.MC	8	77	93	88	72
20. H.MxN	7	92	81	85	80	48. S.MCF	6	70	77	60	66
21. H.MxW	12	92	90	94	82	49. S.MxFS	7	92	86	92	68
22. H.MxWP	7	85	92	78	84	50. S.SC	6	100	78	90	90
23. H.MxWT	6	54	66	27	50	51. S.SR	4	100	100	80	100
24. H.NL	5	42	60	57	100	52. S.ST	4	40	50	20	100
25. H.PD	6	100	73	63	70	53. V.LM	7	85	92	85	66
26. H.PH	6	80	100	80	88	54. V.MxV	6	70	87	90	81
27. H.PN	6	63	100	81	75	55. XUNCL	6	90	100	81	100
28. H.PP	6	100	83	100	100						
Overall accuracy and Kappa value								Accuracy: 85%		Accuracy: 79%	
								Kappa: 0.85		Kappa: 0.79	

SVM support vector machine

RF random forest

PA Producer's accuracy (%)

Conclusions

There was an overall accuracy of 90% for community-level mapping and an 85% accuracy of discriminating 55 species. By doing a minimum noise fraction (MNF) on the data, it removes inherent noise in the hyperspectral data, improves classification accuracy, and reduces the data dimensionality to decrease computational cost. This study concluded that SVM and RF were sensitive to the number of training data and can be the result of high spatial and spectral heterogeneity of the study area. It was also concluded that the number of classes decreased accuracy.

SUMMARY

FIU plans to employ a photogrammetric approach using Unmanned Aerial Vehicles (UAVs) for development of a high resolution (1-m or sub-meter) DEM which will ultimately serve as the stepping stone for development of a regional land surface model of the WIPP site and surrounding basins. This method was favorable considering its affordability, flexibility, and ease of implementation in areas with limited site accessibility. Due to the cost of acquiring and processing LiDAR data for DEM development, the use of unmanned aerial vehicles (UAVs) to acquire digital photos is preferable. The only setback with photogrammetry is that the images acquired by UAVs do not accurately represent the bare earth surface due to the presence of vegetation. FIU therefore conducted this literature review to evaluate methods to identify and remove vegetation from UAV-based photogrammetric point clouds. Machine learning, as of recent, has been used to identify vegetation for the purpose of quantifying vegetation growth as well as for the removal process. Machine learning methods included various classification algorithms such as Support Vector Machines (SVM), and Random Forest, object based image analysis techniques, and Minimum Noise Fraction (MNF) data transformation. Once vegetation has been identified, applicable vegetation removal methods can be applied which include color-based filtering using an excessive greenness vegetation index (VI), Triangulated Irregular Networks (TIN) densification from LAStools, the standard method in Agisoft Photoscan, Iterative Surface Lowering (ISL), a combination of ISL and VI methods, a normalized difference vegetation index (NDVI) and additional algorithms. FIU will determine the most appropriate method to be used based on funding resources, equipment and software availability, and site accessibility.

REFERENCES

- Anders, N., Valente, J., Masselink, R., & Keesstra, S. (2019). Comparing Filtering Techniques for Removing Vegetation from UAV-Based Photogrammetric Point Clouds. *Drones*, 3(3), 61.
- Sadeghi-Tehran, P., Virlet, N., Sabermanesh, K., & Hawkesford, M. J. (2017). Multi-feature machine learning model for automatic segmentation of green fractional vegetation cover for high-throughput field phenotyping. *Plant methods*, 13(1), 103.
- Sandino, J., Gonzalez, F., Mengersen, K., & Gaston, K. J. (2018). UAVs and machine learning revolutionising invasive grass and vegetation surveys in remote arid lands. *Sensors*, 18(2), 605.
- Serifoglu Yilmaz, C., & Gungor, O. (2018). Comparison of the performances of ground filtering algorithms and DTM generation from a UAV-based point cloud. *Geocarto international*, 33(5), 522-537.
- Skarlatos, D., & Vlachos, M. (2018). Vegetation removal from UAV derived DSMS, using combination of RGB and NIR imagery.
- Yilmaz, V., Konakoglu, B., Serifoglu, C., Gungor, O., & Gökalp, E. (2018). Image classification-based ground filtering of point clouds extracted from UAV-based aerial photos. *Geocarto international*, 33(3), 310-320.
- Zhang, C., & Xie, Z. (2013). Object-based vegetation mapping in the Kissimmee River watershed using HyMap data and machine learning techniques. *Wetlands*, 33(2), 233-244.